Solution-Based Straight and Branched CdSe Nanowires

James W. Grebinski,[†] Katherine L. Hull,[‡] Jing Zhang,[§] Thomas H. Kosel,[§] and Masaru Kuno*[,‡]

Department of Chemistry and Biochemistry, Notre Dame Radiation Laboratory, and Department of Electrical Engineering, University of Notre Dame, Notre Dame, Indiana 46556

Received September 4, 2004

Confined straight and branched CdSe nanowires (NWs) are synthesized using a solution-based approach which leverages advances in the synthesis of colloidal CdSe quantum dots (QDs) with incipient approaches for the seeded (solution) synthesis of semiconductor NWs. The resulting straight and branched NWs have typical diameters below 10 nm with accompanying lengths between 1 and 10 μm. In the case of branched NWs, tripod, v-shaped, and y-shaped morphologies are observed. Variations in this preparation lead to higher order structures with multiple arms. The branching transition is discussed, and a possible mechanism based upon geminate NW nucleation is proposed. Such solution-grown straight, branched, and higher-order NWs exhibit potentially interesting optical, electrical, and transport properties due to their narrow radii below the corresponding bulk exciton Bohr radius of CdSe. Furthermore, this transition from straight to branched morphologies opens up avenues for investigating not only size- but also shape-dependent optical/electrical properties of one-dimensional (1D) and quasi-1D materials.

Introduction

Controlling crystallization at the molecular level is an important, yet elusive, goal of materials chemistry. In the broad context of current nanoscience and nanotechnology this interest has materialized into ways for making high-quality semiconductor nanocrystals (NCs) or metal nanoparticles (NPs) with tunable sizes and narrow size distributions. Advances in the synthesis of such particles have led to a basic understanding about crystal nucleation and growth[1] and have also established a wealth of knowledge about their size-dependent optical and electrical properties.[2,3] To this end, the development of high-quality NCs such as CdSe,[4−6] InP,[7,8] and InAs[8,9] has enabled a detailed understanding about the linear absorption and emission of these systems, with remarkable agreement between experiment and theory in explaining subtle observations such as avoided crossings in the absorption[10] and apparent size-dependent emission Stokes shifts.[11] More recently, the realization that a material's optical/electrical properties are dictated by *both* size and shape, has motivated the development of higher-order, quasi-zero-dimensional materials such as nanorods, arrowheads, bipods, tripods, and tetrapods.[12−17]

Within the realm of one-dimensional materials, interest in controlling crystallization dates back to the mid 1960s, with the discovery of vapor−liquid−solid (VLS) growth by Wagner, Ellis, and others.[18,19] In this mechanism, the asymmetric growth of macroscopic semiconductor whiskers is catalyzed by a molten metal particle.[18,19] Renewed interest in VLS has been spurred by the realization that high-quality, size-tunable, metal NPs could, in turn, be used to make semiconductor wires with correspondingly narrow diameters.[20,21] The goal of studying the optical, electrical, and transport properties of quantum confined 1D nanowires (NWs) therefore

* To whom correspondence should be addressed. E-mail: mkuno@nd.edu.

[†] Now affiliated with Department of Chemistry, University of Calgary.

[‡] Department of Chemistry and Biochemistry, Notre Dame Radiation Laboratory.

[§] Department of Electrical Engineering.

(1) Peng, X. *J. Am. Chem. Soc.* **2002**, *124*, 3343. Peng, X.; Wickham, J.; Alivisatos, A. P. *J. Am. Chem. Soc.* **1998**, *120*, 5343.

(2) Yoffe A. D. *Adv. Phys.* **2001**, *50*, 1.

(3) Efros, A. L.; Rosen, M. *Annu. Rev. Mater. Sci.* **2000**, *30*, 475.

(4) Murray, C. B.; Norris, D. J.; Bawendi, M. G. *J. Am. Chem. Soc.* **1993**, *115*, 8706.

(5) Katari, J. E. B.; Colvin, V. L.; Alivisatos, A. P. *J. Phys. Chem.* **1994**, *98* (15), 4109.

(6) Peng, Z. A.; Peng, X. G. *J. Am. Chem. Soc.* **2001**, *123*, 183. Qu, L.; Peng, Z. A.; Peng, X. *Nano. Lett.* **2001**, *1* (6), 333.

(7) Micic, O. I.; Curtis, C. J.; Jones, K. M.; Sprague, J. R.; Nozik, A. J. *J. Phys. Chem.* **1994**, *98* (19), 4966.

(8) Battaglia, D.; Peng, X. *Nano. Lett.* **2002**, *2* (9), 1027.

(9) Guzelian, A. A.; Banin, U.; Kadavanich, A. V.; Peng, X. G.; Alivisatos, A. P. *Appl. Phys. Lett.* **1996**, *69*, 1432.

(10) Norris, D. J.; Bawendi, M. G. *Phys. Rev. B* **1996**, *53*, 16338.

(11) Kuno, M.; Lee, J. K.; Dabbousi, B. O.; Mikulec, F. V.; Bawendi, M. G. *J. Chem. Phys.* **1997**, *106*, 9869.

(12) Peng, X.; Manna, L.; Yang, W.; Wickham, J.; Scher, E.; Kadavanich, A.; Alivisatos, A. P. *Nature* **2000**, *404*, 59.

(13) Kan, S.; Mokari, T.; Rothenberg, E.; Banin, U. *Nat. Mater.* **2003**, *2*, 155.

(14) Schler, E. C.; Manna, L.; Alivisatos, A. P. *Philos. Trans. R. Soc. London A* **2003**, *261*, 241. Manna, L.; Scher, E. C.; Alivisatos, A. P. *J. Am. Chem. Soc.* **2000**, *122*, 12700. Manna, L.; Milliron, D. J.; Meisel, A.; Scher, E. C.; Alivisatos, A. P. *Nat. Mater.* **2003**, *2*, 382.

(15) Yu, W. W.; Wang, Y. A.; Peng, X. G. *Chem. Mater.* **2003**, *15*, 4300.

(16) Jun, Y. W.; Lee, S. M.; Kang, N. J.; Cheon, J. *J. Am. Chem. Soc.* **2001**, *123*, 5150.

(17) Chen, M.; Xie, Y.; Lu, J.; Xiong, Y.; Zhang, S.; Qian, Y.; Liu, X. *J. Mater. Chem.* **2002**, *12*, 748.

(18) Wagner, R. S.; Ellis, W. C. *App. Phys. Lett.* **1964**, *4* (5), 89. Wagner, R. S.; Ellis, W. C.; Jackson, K. A.; Arnold, S. M. *J. Appl. Phys.* **1964**, *35* (10), 2993. Wagner, R. S. VLS Mechanism of Crystal Growth. In *Whisker Technology*; Levitt, A. P., Ed.; Wiley: New York, 1970.

(19) Givargizov, E. I. *J. Cryst. Growth* **1975**, *31*, 20. Givargizov, E. I. In *Current Topics in Materials Science;* Kaldis, E., Ed.; North-Holland: Amsterdam, 1978; Vol. 1, Chapter 3.

(20) Wu, Y.; Yan, H. Q.; Huang, M.; Messer, B.; Song J. H.; Yang, P. D. *Chem. Eur. J.* **2002**, *8* (6), 1261.

10.1021/cm048498h CCC: $27.50
Published on Web 11/17/2004

appears at hand. However, major challenges still include the controlled (regular) synthesis of NWs with diameters smaller than the corresponding bulk exciton Bohr radius. Additional issues, likely to be of future concern, entail manipulating not only the diameter but also the *shape* of the NWs in order to study their morphology-dependent optical and electrical properties.

Incipient approaches for making semiconductor NWs encompass traditional VLS growth, which utilizes chemically synthesized, size-selected metal NPs,[20,21] as well as variations that employ laser-ablated species.[22] Effort has also been directed toward alternative solution-based approaches that include solution−liquid−solid (SLS)[23] and supercritical-fluid−liquid−solid (SFLS) growth.[24] All schemes ultimately rely on a metal catalyst particle for promoting NW growth. However, in the case of a SLS mechanism, the metal NP must have a melting point capable of being attained by solution chemistry.[23] Catalyst elements are therefore restricted to common low-melting species such as In, Sn, Bi, and Ga. Unfortunately, few preparations exist for high-quality NPs of these elements, let alone those with narrow size distributions. While procedures do exist for synthesizing NPs of In,[25,26] Sn,[27,28] and Bi[29−31] they typically yield particles with diameters on the order of tens of nanometers, rendering them unsuitable, on first inspection, for promoting the growth of NWs capable of exhibiting quantum confinement effects. To overcome this limitation, a template-mediated approach can be utilized to first synthesize (nanometer sized, narrow size distribution) particles of elements such as Au, whereupon a shell of a desired low-melting substance can be deposited onto its surface giving bimetallic particles. Such core/shell species are effectively NPs of the low-melting element because of their large surface-to-volume ratio. In this manner, SLS compatible particles whose size distributions are dictated by the initial core NP distribution can be readily obtained.[32]

The current work describes such a solution-based approach that yields both straight and branched CdSe NWs capable of exhibiting quantum confinement effects. By varying the apparent Cd/Se ratio of the preparation and/or excess amount of trioctylphosphine ligand, straight and branched NWs with v-shaped, y-shaped, and tripod morphologies are obtained. In the case of branched NWs, a geminate nucleation mechanism is thought to be responsible for the branching, with variations in the Cd/Se ratio dictating this straight to branched transition. Resulting NW diameters are at or below 10 nm with lengths ranging from 1 to 10 μm. The NWs are crystalline and, in turn, exhibit quantum confinement effects in their absorption spectra. The present NWs, as well as other related systems,[33−35] represent new 1D materials that can be investigated for both size- and shape-dependent optical and electrical properties. The current study also advances CdSe as a model system with which to study the evolution of these properties with size, shape, and dimensionality.

Experimental

Materials. The solvents toluene, methanol, and acetonitrile were all used as received from Fisher Scientific. In the preparation of Au NPs, hydrogen tetrachloroaurate(III) trihydrate ($HAuCl_4 \cdot 3H_2O$, Acros), tetra-*n*-octylammonium bromide (TOAB, 99% Acros), and sodium borohydride ($NaBH_4$, 99% Acros) were stored in a desiccator and used as received. To prepare Au/Bi core/shell NPs, both phenyl ether [Ph_2O, 99% Acros] and trioctylphosphine (TOP, 90% Aldrich) were flushed with N_2 and stored in a glovebox. Triethyl bismuth[36] ($Bi(Et)_3$, CAS 617-77-6, Organometallics) was filtered through a 0.2-μm PTFE filter and stored in a glovebox freezer. To prepare straight and branched CdSe NWs, trioctylphosphine oxide (TOPO, 90% Strem), trioctylphosphine (TOP, 90% Aldrich), selenium powder (99% Aldrich), octanoic acid (98% Lancaster), and cadmium oxide (CdO, 99% Aldrich) were all purchased and used as received. Solutions of trioctylphosphine selenide (TOPSe), with concentrations ranging from 0.5 to 2.0 M, were prepared by mixing elemental Se (0.197−0.790 g, 2.50−10.0 mmol) with TOP (5.00 mL, 11.2 mmol).[4]

Preparation of Au/Bi Catalyst NPs. Au/Bi catalyst NPs were synthesized using an approach described in ref 37. Briefly, the procedure entailed mixing a solution of hydrogen tetrachloroaurate (III) trihydrate (0.125 g, 0.317 mmol) in (6.25 mL) deionized water with a phase-transfer solution consisting of tetra-*n*-octylammonium bromide (0.200 g, 0.366 mmol) in (8.125 mL) toluene. After transfer of the gold ions into the organic phase, a solution of TOP (0.100 mL, 0.220 mmol) in (2.00 mL) toluene was then injected into this solution. A dramatic color change from clear to bright red occurred, whereupon additional TOP was added (dropwise) until the solution turned milky white from light scattering. The resulting mixture was then stirred for ∼5−10 min. To complete the reaction, an injection solution containing $NaBH_4$ (44.0 mg, 1.16 mmol) in water (5.00 mL) was subsequently added with a syringe pump at a nominal rate of 7 mL/hr. After adding the reducing agent, the organic phase was separated and the Au NPs were precipitated with methanol. The suspension could then be centrifuged to recover a NP solid, which can subsequently redissolved in toluene. The resulting Au NPs had an average diameter of 1.5 nm with an accompanying ensemble size distribution of ∼18%.[37]

Subsequent surface passivation of Au NPs with elemental bismuth was achieved through the thermolysis of triethylbis-

(21) Gudiksen, M. S.; Wang, J.; Lieber, C. M. *J. Phys. Chem. B* **2001**, *105*, 4062. Lauhon, L. J.; Gudiksen, M. S.; Wang, D.; Lieber, C. M. *Nature* **2002**, *420*, 57. Gudiksen, M. S.; Lauhon, L. J.; Wang, J.; Smith, D. C.; Lieber, C. M. *Nature* **2002**, *415*, 617.

(22) Morales, A. M.; Lieber, C. M. *Science* **1998**, *279*, 208.

(23) Trentler, T. J.; Hickman, K. M.; Goel, S. C.; Viano, A. M.; Gibbons, P. C.; Buhro, W. E. *Science* **1995**, *270*, 1791. Yu, H.; Buhro, W. E. *Adv. Mater.* **2003**, *15* (5), 416. Yu, H.; Li, J. B.; Loomis, R. A.; Wang, L. W.; Buhro, W. E. *Nat. Mater.* **2003**, *2* (8), 517. Trentler, T. J.; Goel, S. C.; Hickman, K. M.; Viano, A. M.; Chiang, M. Y.; Beatty, A. M.; Gibbons, P. C.; Buhro, W. E. *J. Am. Chem. Soc.* **1997**, *119* (9), 2172. Yu H.; Li, J.; Loomis, R. A.; Gibbons, P. C.; Wang, L. W.; Buhro, W. E. *J. Am. Chem. Soc.* **2003**, *124* (17), 16168.

(24) Holmes, J. D.; Johnston, K. P.; Doty, R. C.; Korgel, B. A. *Science* **2000**, *287*, 1471. Hanrath, T.; Korgel, B. A. *J. Am. Chem. Soc.* **2002**, *124*, 1424.

(25) Zhao, Y.; Zhang, Z.; Dang, H. *J. Phys. Chem. B* **2003**, *107*, 7574.

(26) Nedeljkovic, J. M.; Micic, O. I.; Ahrenkiel, S. P.; Miedaner, A.; Nozik, A. J. *J. Am. Chem. Soc.* **2004**, *126*, 2632.

(27) Bonnerman, H.; Brijoux, W.; Joussen, T. *Angew. Chem., Int. Ed. Engl.* **1990**, *29*, 273.

(28) Nayral, C.; Viala, E.; Fau, P.; Senocq, F.; Jumas, J. C.; Maisonnat, A.; Chaudret, B. *Chem. Eur. J.* **2000**, *6* (22), 4082.

(29) Gutierrez, M.; Henglein, A. *J. Phys. Chem.* **1996**, *100*, 7656.

(30) Fang, J.; Stokes, K. L.; Wiemann, J. A.; Zhou, W., L.; Dai, J.; Chen, F.; O'Connor, C. J. *Mater. Sci. Eng., B* **2001**, *83*, 254.

(31) Foos, E. E.; Stroud, R. M.; Berry, A. D.; Snow, A. W.; Armistead, J. P. *J. Am. Chem. Soc.* **2000**, *122*, 7114.

(32) Yu, H.; Gibbons, P. C.; Kelton, K. F.; Buhro, W. E. *J. Am. Chem. Soc.* **2001**, *123*, 9198.

(33) Wang, D.; Fang, Q.; Yang, C.; Zhoung, Z.; Lieber, C. M. *Nano Lett.* **2004**, *4*, 871.

(34) Dick, K. M.; Deppert, K.; Larsson, M. W.; Martensson, T.; Seifert, W.; Wallenberg, L. R.; Samuelson, L. *Nat. Mater.* **2004**, *3*, 380.

(35) Wu, Z. H.; Mei, X.; Kim, D.; Blumin, M.; Ruda H. E.; Liu, J. Q.; Cavinagh, K. L. *Appl. Phys. Lett.* **2003**, *83*, 3368.

(36) Mitzi, D. B. *Inorg. Chem.* **1996**, *35*, 7614.

(37) Grebinski, J. G.; Richter, K. L.; Zhang, J.; Kosel, T. H.; Kuno, M. *J. Phys. Chem. B* **2004**, 108, 9745.

muth in the presence of a mildly coordinating solvent. To this end, a mixture of phenyl ether (4.00 mL, 25.2 mmol), TOP (0.600 mL, 1.34 mmol), and 1/4 of the above Au NP preparation was added to a three-neck flask. This mixture was then heated to 100 °C under vacuum to dry and degas the reagents. In a glovebox, an injection solution containing phenyl ether (4.00 mL, 25.2 mmol), TOP (0.600 mL, 1.34 mmol), and $Bi(Et)_3$ (20.0−150 μL, 0.123−0.922 mmol) was prepared. Prior to adding the $Bi(Et)_3$ solution, the reaction flask was backfilled with N_2, whereupon the injection mixture was delivered with a syringe pump at a nominal rate of 7 mL/hr. After addition, the solution was allowed to cool to room temperature, and the resulting Au/Bi NPs were precipitated with acetonitrile. Care was taken to prevent adding an excess of the polar aprotic as this leads to a phase separation, which complicates recovery of the NPs. The suspension was then centrifuged at 4400 rpm for 10 min to obtain a NP precipitate which was redissolved in toluene along with a few drops of oleic acid (~0.070 mmols). This solution was stored in a glovebox freezer where it keeps for several months with no adverse effects on the NW syntheses.[37]

Concentrations of all Au/Bi catalyst NP solutions were normalized to an absorbance value of $A = 0.1260$ at 500 nm, yielding an estimated NP stock concentration of ~0.38 mM.[37] Although this absorbance is empirical, the choice of wavelength is intentional. Since bismuth has a plasmon resonance below 400 nm[29,30] absorbances above this wavelength are likely due to the Au NPs alone and are consequently independent of the Bi overcoating thickness. In this fashion, Au/Bi NP concentrations can be standardized between different Au NP preparations and Bi overcoatings.

Synthesis of Straight NWs. A mixture consisting of TOPO (3.00 g, 7.76 mmol), CdO (25.0 mg, 0.194 mmol), and octanoic acid (0.23 mL, 1.43 mmol) was heated to 100 °C under vacuum to dry and degas the reagents. When complete, the reaction vessel was backfilled with N_2, and the orange/red slurry was heated to 330 °C. The solution progressively cleared as CdO reacted with octanoic acid. A minimum 2.5:1 mole ratio of octanoic acid to Cd was used to ensure complete transformation of the initial precursor. In a glovebox, an injection solution consisting of standardized ~1.4 nm (30.0 μL, 0.184 mmol $BiEt_3$) Au/Bi NPs (175 μL, ~0.460 mol) and 1.0 M TOPSe (25.0 μL, 25.0 μmol) was prepared. This solution was then injected into the reaction mixture at 330 °C to initiate the reaction. A rapid color change occurred, after which the resulting dark red/brown solution was briefly kept at high temperatures before cooling. Toluene was then added to prevent TOPO from solidifying, and the reaction mixture was centrifuged to remove any precipitated material. The supernantant containing the product was retained, with the synthesized NWs indefinitely stable in this form. However, short chain alcohols such as methanol, ethanol, 2-propanol, or butanol can be added to precipitate the NWs. Although methanol and ethanol are suitable nonsolvents, longer chain alcohols are preferred as they induce a gentler precipitation, which suppresses NW bundling and the extraction of any impurity CdSe quantum dots (QDs) produced during the reaction. The recovered NWs can subsequently be resuspended in common organic solvents such as toluene, with varying degrees of stability depending upon the amount of excess surfactant present.

Manipulating the cadmium-coordinating ligand provides partial access to the size and morphology of the resulting NWs. However, ligand selection alone does not allow fine control over these parameters. In this respect, altering the Cd-coordinating species results in dramatic variations of the NW diameter, overall degree of branching, and apparent quality. For example, tetradecylphosphonic acid (TDPA) generally retards NW growth, yielding a mixture of nanorods, irregular nanostructures, and occasional NWs. By contrast, use of hexylphosphonic acid (HPA) leads to uncontrolled growth, and eventual precipitation of larger-diameter straight and branched NWs. Empirically, octanoic acid has been found to provide the best control over the growth kinetics of both straight and branched NW preparations and is the Cd-coordinating surfactant of choice unless otherwise noted.

Synthesis of Branched NWs. The synthesis of branched CdSe NWs is conducted in a fashion analogous to that of straight NWs. A mixture consisting of TOPO (2.50 g, 6.47 mmol), CdO (17.5 mg, 0.136 mmol), and octanoic acid (0.160 mL, 0.997 mmol) was heated to 100 °C under vacuum to dry and degas the reagents. After this, the reaction vessel was backfilled with N_2 and heated to 330 °C. In a glovebox, an injection solution consisting of standardized ~2.2 nm (50.0 μL, 0.307 mmol $BiEt_3$) Au/Bi NPs (175 μL, ~0.460 mol), and 2.0 M TOPSe (40.0 μL, 80.0 μmol) was prepared. This solution was then injected into the reaction mixture at 330 °C to initiate the reaction. Resulting branched NWs were then recovered in a manner equivalent to that described above. Solubility in common organic solvents such as toluene is analogous to that of straight NWs and again varies with the amount of excess surfactant present. To further increase branching, neat TOP (0.400 mL, 0.893 mmol) was added to the above reaction mixture prior to injecting the Au/Bi NPs/TOPSe precursor. This yielded preparations where nearly all NWs exhibited some form of branching.

Control Experiments. To test whether straight or branched NWs can be grown without a catalyst, control experiments were conducted without Au/Bi NPs. In such experiments, only CdSe QDs were obtained, establishing the need for a Au/Bi precursor. Additional control experiments were conducted to see whether NWs could be grown using triethylbismuth alone. To this end, $BiEt_3$ (230 μL, 1.41 mmol) and TOPSe (1.0 M, 25.0 μL, 25.0 mmol) were injected into a straight/branched NW reaction mixture. A dark gray precipitate, free of NWs, resulted, illustrating that under the described conditions, the (in situ) self-nucleation of Bi NPs/particles does not efficiently catalyze the growth of either straight or branched NWs.

Instrumentation. Samples for low- and high-resolution transmission electron microscopy (TEM) analysis were prepared by dropping a dilute toluene solution of NWs onto ultrathin carbon-coated copper grids (Ladd) and wicking off the excess. Survey TEMs were conducted during the synthesis of straight and branched CdSe NWs using a JEOL JEM-100SX electron microscope. Low-resolution TEM micrographs were taken with either a Hitachi H-600 or JEOL-2010 electron microscope. High-resolution TEM micrographs were taken exclusively with a JEOL-2010 TEM. UV−visible absorption experiments were conducted with a Cary 50-Bio UV−visible spectrophotometer. Wide-angle X-ray diffraction (XRD) samples were prepared by precipitating straight/branched CdSe NWs from the growth solution with small amounts of 2-propanol, followed by multiple washings with acetone to remove any excess surfactant. Samples were dried under vacuum, resuspended in <1 mL of acetone, and allowed to dry on a quartz single-crystal (0001) off-axis substrate. XRD scans were collected using a Bruker D8 Advance X-ray diffractometer using Cu Kα ($\lambda = 1.54$ Å) radiation. Ensemble energy-dispersive X-ray spectroscopy (EDXS) samples were prepared in the same manner as XRD samples, placed onto conductive carbon tape, and mounted onto a scanning electron microscope (SEM) sample holder. EDXS measurements were obtained with a JEOL JXA-8600 super microprobe operating at an accelerating voltage of 15 kV. Additional TEM-based EDXS measurements were carried out using a JEOL-2010F electron microscope with specimens supported on lacy carbon substrates (Ladd).

Results and Discussion

CdSe has, over the last 20 years, been one of the most extensively studied semiconductor systems in nanoscale form.[1−6,10,11] Numerous studies have focused on the size-dependent properties of high-quality colloidal CdSe QDs.[2,3,10,11] Recent work, however, has emphasized the development of CdSe NRs and other quasi-zero-dimensional (0D) materials through the manipulation of reaction conditions, Cd-coordinating ligands, and/or growth kinetics.[12,14] Such trends reflect the realization that the properties of nanoscale materials are influenced

not only by size and dimensionality, but also by shape. Thus, the evolution of CdSe as a model system through which the physical, optical, and electrical properties of nanoscale materials (from 0D to 1D) can be studied is unprecedented. The syntheses described herein add to this growing body of knowledge by expanding the opportunities for studying the mesoscopic properties of CdSe in the limit of one-dimensional (1D) straight *and* quasi-1D branched NWs.

A solution-based approach for the seeded growth of CdSe NWs is pursued since this technique leverages advances in the synthesis of high-quality colloidal QDs[1,4−6] with incipient approaches for generating solution-based semiconductor NWs.[23,37] Benefits of such a strategy over more traditional VLS growth include the following: lower reaction temperatures, potentially higher yields, and ultimately, soluble material whose surface functionalization can be investigated. This hybrid approach has also yielded some of the narrowest NWs to date with radii below a material's corresponding bulk exciton Bohr radius.[23,37]

What follows is a general discussion about major synthetic parameters involved in the synthesis of straight and branched CdSe NWs. Since their solution chemistry encompasses various competing kinetics as well as growth regimes, the trends established provide useful, predictive guidelines for optimizing this as well as other analogous NW preparations. In the current case, the basis for such syntheses is a seeded growth mechanism[23] whereby a molten metal NP is saturated with Cd/Se through the thermolysis of simple organometallic precursors. Upon supersaturation, CdSe nucleates on the NP surface, forming the core of a growing NW.[38] This segment then grows outward from the NP by the addition of Cd and Se ions dissolved within the Au/Bi catalyst. Variations in the concentration of the reaction mixture, temperature, initial Cd/Se ratio, Au/Bi size, Au/Bi volume, and the presence of excess TOP *all* influence the morphology of the resulting CdSe NWs. A discussion of their effects is provided below.

Synthetic Considerations. *Reaction Mixture Concentration.* In either straight or branched NW preparations, diluting the reaction mixture by increasing the TOPO content promotes the growth of straighter NWs. This likely originates from an overall decrease in selenium concentration within the immediate vicinity of a Au/Bi NP, favoring the nucleation of straight over branched NWs (proposed mechanism described below). In addition, altering the concentration of the reaction mixture delays saturation of the NP, producing a competition between catalyzed and uncatalyzed growth, as well as self-nucleation. For example, diluting the reaction mixture causes an increase of the NW diameter, highlighting an interplay between catalyzed (longitudinal) and uncatalyzed (transverse) NW growth. Conversely, concentrating the reaction mixture shifts the growth kinetics toward a regime where CdSe self-nucleation dominates catalyzed growth, yielding QDs rather than NWs. An optimal dilution for obtaining narrow, straight/branched NWs is therefore empirically determined. These two limits illustrate the different growth modes underlying a solution-based NW preparation.

Reaction Temperature. Both straight and branched CdSe NWs are grown at temperatures between 250 and 350 °C. Empirically, straight NWs are grown at temperatures between 330 and 350 °C, while branched NWs are grown at slightly lower temperatures (280−330 °C). When either reaction is carried out at the high end of its respective temperature range less overall branching is generally seen. Conversely, when straight/branched preparations are conducted at the lower end of their temperature range, modest increases in branching are observed. This suggests that while NW growth is kinetically driven, branching may encompass additional thermodynamic considerations.

The 250−280 °C temperature range (or below) is rarely utilized in either straight or branched NW preparations because at these temperatures all wires exhibit significant surface roughness. A possible explanation may involve zinc blende (ZB)/wurtzite (W) twinning and/or ZB/W admixtures since all NWs exhibit ZB and W sections (discussed below). In this respect, zinc blende is predicted to be the most stable phase of CdSe.[39] Syntheses conducted at lower temperatures may therefore yield NWs with increased ZB character; likewise, those grown at higher temperature may exhibit more W character.

Unfortunately, this temperature-dependent ZB/W ratio is difficult to verify via ensemble powder XRD measurements, due to NW orientation induced by wires lying flat on the substrate. As discussed later, the resulting crystallographic texture suppresses key ZB and W X-ray reflections (Figure 7), complicating a quantitative analysis of the NW ZB/W ratio. Complementary selected area diffraction (SAD) experiments using TEM also cannot quantify the ZB/W ratio, due to overlapping spots from both phases. Additional autocorrelation analyses (Supporting Information) of the ZB/W twinning through its contrast in TEM micrographs show no periodicity of either W or ZB regions, indicating that they occur randomly. Thus, a definitive assessment of a potential temperature-dependent ZB/W ratio cannot be made and must wait for more detailed experiments. However, the enhanced branching at lower temperatures as well as TEM observations indicating the importance of the ZB phase in branching are both suggestive of the above hypothesis.

Apparent Cd:Se Ratio. In practice, straight NWs are obtained using Cd rich conditions with a nominal Cd/Se ratio of ∼7:1 (Experimental Section). Increasing this ratio by decreasing the molarity of the TOPSe precursor (constant volume) yields NWs with successively larger diameters. All straight NW preparations are therefore initiated with Cd/Se ratios of ∼7:1. On the other hand, increasing the selenium content of a preparation noticeably increases branching. Investigations into this effect have led to branched NW preparations (Experimental Section) with initial Cd/Se ratios that approach 1:1 (1.70:1).

(38) The Bi−Cd−Se ternary phase diagram shows a eutectic temperature of 265 °C (just below the bulk Bi melting temperature of 271 °C) across the entire composition range with the eutectic point at 4 atomic percent CdSe. *Handbook of Ternary Alloy Phase Diagrams*; Villars, P., Prince, A., Okamoto, H., Eds.; ASM International: Materials Park, OH, 1997; Vol. 5.

(39) Yeh, C. Y.; Lu, Z. W.; Froyen, S.; Zunger, A. *Phys. Rev. B* **1992**, *46*, 10086.

An increase in selenium content can be accomplished by increasing the molarity of the TOPSe precursor (fixed volume). Thus, TOPSe solutions with concentrations up to 2.0−2.2 M can be made.[4] Additional branching can be induced by increasing both the molarity of the TOPSe precursor and its injected volume. However, a point is quickly reached beyond which increasing the TOPSe volume causes no further increase in branching and simultaneously enlarges the observed NW diameter. This suggests that under Se rich conditions, uncatalyzed (transverse) growth competes with catalyzed (longitudinal) growth, adding to the NW width rather than its length. Although additional branching can be obtained by lowering the CdO content, decreasing it beyond 0.010 g (0.078 mmol) yields no additional branching and comes at the expense of increased NW diameters. Optimal Cd/Se ratios of ∼7:1 for straight and ∼1.7:1 for branched CdSe NWs are therefore found.

Au/Bi NP Size. Au/Bi NP diameters generally range from 1.4 to 3.0 nm.[37] Resulting size distributions are on the order of 20%, in line with initial Au NP distributions.[37] All Au/Bi sizes between 1.4 and 3.0 nm catalyze the growth of straight and branched CdSe NWs. However, differences are observed with size, leading to variations in the resulting NW diameters, the degree of residual branching in straight NW preparations, and in some cases, the optimal temperature for attaining branched growth.

Qualitatively, when ∼2.2 nm (50 μL, 0.307 mmol, $BiEt_3$) Au/Bi NPs are used in straight/branched preparations, NW diameters range from 5 to 7 nm. These widths increase to 7−10 nm when ∼2.3−2.5 nm (75−100 μL, 0.461−0.615 mmol $BiEt_3$) Au/Bi NPs are employed. Average NW diameters further increase to ∼12−13 nm when ∼2.7 nm (120 μL, 0.737 mmol $BiEt_3$) particles are used, and even larger widths (∼15 nm) are obtained with ∼2.8−3.0 nm (150 μL, 0.922 mmol $BiEt_3$) Au/Bi NPs. In all cases, the size of the catalyst does not influence the width of resulting NW diameter distributions.

The NP size also influences the morphology of the NWs. Empirically, employing larger Au/Bi NPs in straight NW preparations decreases residual branching when the number of introduced particles is kept constant. This is best highlighted by the fact that ∼2.5 and ∼2.7 nm Au/Bi NPs yield noticeably less residual branching than in analogous preparations carried out with ∼1.4 to ∼2.2 nm Au/Bi NPs. A possible explanation may lie in an unintentional Bi induced Se deficiency caused by the appearance of Bi_2Se_3 in NPs with larger Bi overcoatings.[40,41] By contrast, the degree of branching in actual branched NW preparations decreases when very small Au/Bi particles are used, forcing higher reaction temperatures (∼330 °C) to recover some of this lost branching. This suggests a threshold Au/Bi NP size (∼2.2 nm) below which branching, in general, becomes inefficient.

Au/Bi NP Volume. The effect of catalyst volume on both straight and branched NW growth can be probed by standardizing the concentrations of different Au/Bi sizes (Experimental Section). Volumes between 175 and 500 μL (∼0.460−1.32 mol) have been tested to determine their effects on both NW growth kinetics and NW morphology. When small (100−175 μL, ∼0.263−0.460 mol) amounts of Au/Bi NPs are used, QDs rather than NWs are obtained. This can be understood as insufficient NPs in the reaction mixture to effectively compete with the self-nucleation of colloidal CdSe QDs. Conversely, when large amounts of Au/Bi NPs are used (>500 μL, ∼1.32 mol), a precipitate consisting of irregular Au/Bi aggregates is observed. For all NP sizes, the volume range between 175 and 350 μL (∼0.460−0.921 mol) is found to be optimal for growing either straight or branched NWs.

Additional relationships are observed between the volume of Au/Bi NPs used and the resulting NW length and/or degree of branching. Small amounts of Au/Bi precursor (∼100 μL, ∼0.263 mol) yield short NWs. When catalyst volumes increase to 175−350 μL (∼0.460−0.921 mol), NW lengths increase in tandem. Beyond this, NW lengths again shorten and simultaneously become thicker by a factor of ∼2, with less residual branching in straight NW preparations. This behavior highlights both the self-nucleation of CdSe QDs and Au/Bi aggregates (described above), as well as a competition between catalyzed (longitudinal) and uncatalyzed (transverse) NW growth. Analogous behavior can be seen with different Au/Bi NP sizes.

TOP Doping and Other Modifications. Dramatic changes are observed when a small amount of TOP is mixed with TOPO under either straight or branched reaction conditions. For instance, when 0.100 mL (0.220 mmol) of TOP is added to a branched NW preparation, most, if not all, NWs exhibit branching with a noticeable increase in the number of higher order structures (Figure 9). Additional TOP doping enhances this effect, but also leads to an increase in NW precipitation during the reaction. Doping has also been conducted with hexadecylamine (HDA), another mildly coordinating surfactant compatible with TOPO. Preliminary results, however, reveal no increase in NW branching, suggesting a ligand specificity to the effect. Identical behavior is observed in preparations conducted under straight NW conditions. Although the role of TOP is not understood, the doping of a branched NW reaction has currently been optimized at 0.400 mL (0.893 mmol) TOP to maximize branching while minimizing precipitation (Experimental Section). It should be noted, however, that while the apparent Cd/Se ratio of the preparation is currently thought to dictate the appearance of branching, the obvious role of excess TOP in promoting branching should not be overlooked as a potential cause of branching. This would be in line with recent studies on quasi zero-dimensional structures such as tetrapods where ligand binding to specific crystal faces is thought to aid the formation of branched structures.[14,15]

Specifics. Under the general conditions described above and more specifically in the Experimental Section, the following results are obtained from the synthesis of straight and branched CdSe NWs. Figure 1(a−d) show both low- and high-resolution TEM images of representative CdSe NWs made using a straight NW synthesis. An ensemble of wires with an average diameter (stan-

(40) Moffart, W. G. *The Handbook of Binary Phase Diagrams*; General Electric Co.: Schenectady, NY, 1984.

(41) Wang, W.; Geng, Y.; Qian, Y.; Xie, Y.; Liu, X. *Mater. Res. Bull.* **1999**, *34*, 131. Harpeness, R.; Gedanken, A. *New J. Chem.* **2003**, *27*, 1191. Li, Y.; Wang, Z.; Ding, Y. *Inorg. Chem.* **1999**, *38*, 4737.

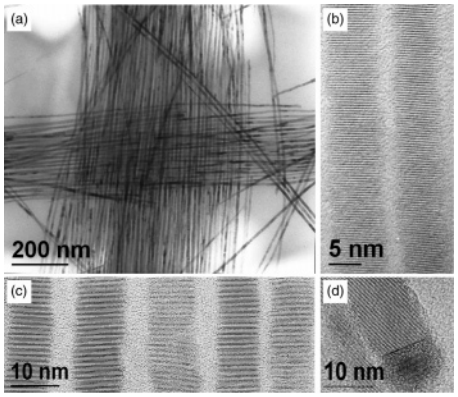

Figure 1. (a) Low-resolution TEM micrograph of a straight NW ensemble. (b) High-resolution TEM micrograph of two adjacent thin (~7−8 nm) NWs. (c) High-resolution TEM micrograph of five adjacent thick (~9−10 nm) NWs. (d) High-resolution TEM micrograph of a straight NW end revealing the Au/Bi catalyst particle and a flat interface.

dard deviation) of 10 (3) nm and lengths between 1 and 10 μm is shown in Figure 1a, demonstrating the procedure's ability to produce high-quality CdSe NWs. Figure 1b shows a high-resolution TEM (HRTEM) micrograph of narrow (~7 nm diameter) NWs. Such wires can be made using small Au/Bi NPs with mean diameters between 1.4 and 2.0 nm; larger NWs are made with correspondingly larger catalyst particles. The HRTEM micrograph in Figure 1c shows a group of thicker (~10 nm diameter) wires made using ~2.5 nm Au/Bi NPs. All TEM micrographs demonstrate the high degree of crystallinity, narrow diameters, smooth surfaces, and narrow size distributions of the solution-based NWs.

In the case of thick NWs with typical diameters at or above 10 nm (Figure 1c), a Au/Bi NP is occasionally retained at the end of the wire. Figure 1d illustrates an example of this, which is of particular interest given that both NW and NP show lattice fringes. More specifically, the NP appears to exhibit a crystalline core/nanocrystalline shell morphology that is consistent with the use of bimetallic core/shell particles in the synthesis. Also notable is the flat interface between the NP and the NW. Such flat ends are often seen in wires where the catalyst has fallen off during post-synthesis processing, although such blunt interfaces may also arise from fracturing of the wire during this step. By contrast, the complementary ends of these NWs are generally pointed suggesting that they nucleate and emerge from the catalyst particle first. Figure 2a illustrates an example of a straight NW with both pointed and blunt ends. Furthermore a cartoon depicting the idealized growth of a NW is illustrated in Figure 2b to motivate the explanation for such blunt and pointed NW ends. In all cases, the observation of Au/Bi NPs attached to NW ends suggests a seeded growth mechanism[20−23] that is corroborated by control experiments showing no NW growth in the absence of Au/Bi NPs. Although such particles are rarely seen attached to thinner (<10 nm diameter) NWs, the seeded growth mechanism is expected to apply to these wires as well.

All NWs exhibit twinning in ZB sections of the wire.[23,37] This admixture likely arises from the low energy difference between the two crystal phases and minor structural changes associated with transitions

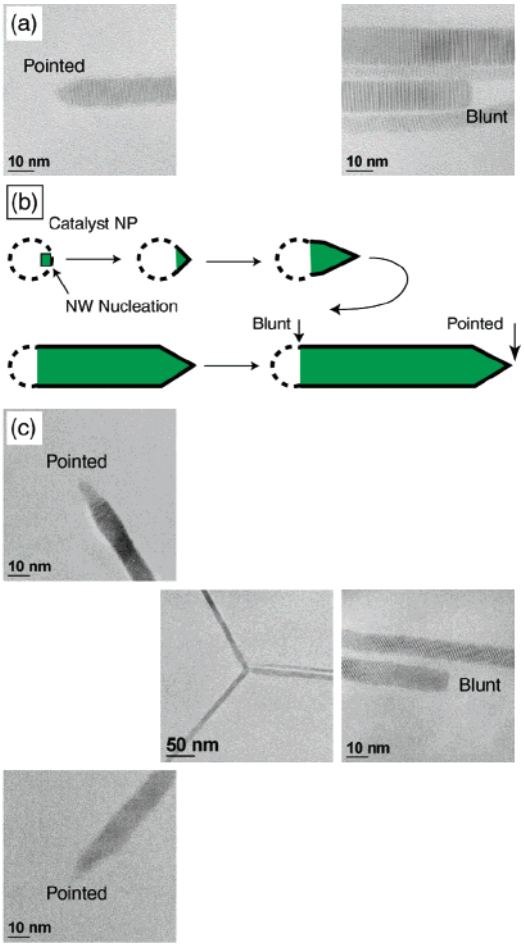

Figure 2. (a) High-resolution TEM micrographs of two ends of a straight NW showing pointed and blunt faces. (b) Cartoon schematic to motivate the appearance of pointed and blunt NW ends. (c) High-resolution TEM micrograph of all three ends of a tripod NW.

from eclipsed to staggered conformations.[39] To this end, polytypism has been observed in CdSe tetrapods, where the core is notably ZB and W arms grow out of equivalent {111} ZB faces.[14] Mixed-phase crystals are also observed in CdSe NRs, suggesting a commonality of this phenomenon in CdSe.[14] An autocorrelation analysis of the NW twinning through its TEM contrast shows no periodicity to either ZB or W sections, indicating random occurrences rather than any apparent polytypism (Supporting Information).

To demonstrate twinning, a wire model was constructed with a growth axis along the ⟨111⟩ and ⟨0001⟩ directions of the ZB and W phases, respectively. This model is illustrated in Figure 3a, where each of the two adjacent ZB segments of the wire appears as a pattern of distorted hexagons when viewed down ⟨110⟩ directions normal to the growth axis. These segments are in a FCC twin orientation relationship, with the twin boundary T denoted by a solid vertical line along the (111) plane normal to the wire axis; this twin boundary has the same structure as a single layer of wurtzite. The solid line B represents the interphase boundary between the central ZB and rightmost W segment of the model. Because of twin boundaries in ZB sections, experimental lattice images of ⟨110⟩ oriented NWs are expected to exhibit a characteristic "zigzag" pattern of the {111} planes (outlined by the dashed lines in Figure 3a) which

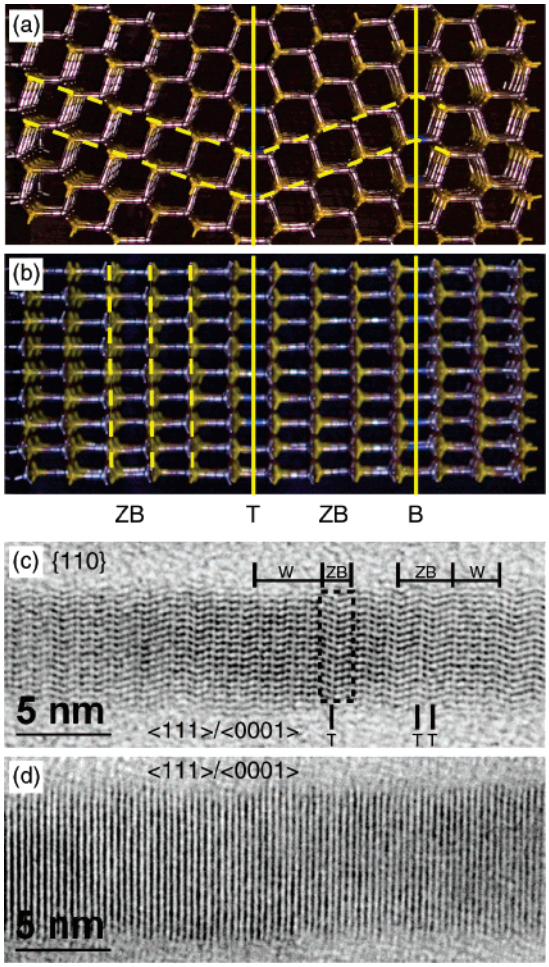

Figure 3. Color photograph of a twinned NW model grown along the ⟨111⟩/⟨0001⟩ direction. Zinc blende and wurtzite regions of the NW are denoted by ZB and W, respectively. T denotes a twin boundary between two ZB segments of different orientation, and B is a phase boundary between a ZB and a W segment. (a) Viewed down ⟨110⟩ directions normal to the growth axis. (b) Viewed down a ⟨112⟩ direction. (c) HRTEM micrograph of a CdSe NW viewed down ⟨110⟩ directions. Selected twin boundaries (T) as well as ZB and W sections are highlighted. (d) HRTEM micrograph of a CdSe NW viewed down an intermediate direction between ⟨110⟩ and ⟨112⟩.

are inclined relative to the wire axis. Figure 3c is an actual example taken from HRTEM micrographs of CdSe NWs where one of many twin boundaries (T) in the specific NW is enclosed by a dashed rectangular box.

When the twinned wire model in Figure 3a is rotated about the growth axis so that the viewing direction is not ⟨110⟩, the ZB/W twinning is no longer apparent. More specifically, a dramatic change occurs in the expected experimental lattice pattern, where instead of zigzags, only parallel lattice fringes are predicted (Figure 3b, vertical dashed lines). An actual instance of this situation is shown in Figure 3d where a wire is viewed down a direction intermediate between ⟨110⟩ and ⟨112⟩; additional examples are seen in Figure 1b, c, and d. Since there exist a finite number of ⟨110⟩ directions, straight NWs are commonly viewed down non ⟨110⟩ directions. Hence, most wires observed in TEM experiments exhibit parallel rather than zigzag lattice fringes; these are the (111) planes in ZB sections, and (0001) planes in W sections. Additional TEM analyses, however, suggest that all NWs exhibit twinning.

By manipulating the Cd/Se ratio, as well as other synthetic parameters, a transition from straight to branched NW morphologies is achieved. Whereas straight NW preparations have Cd/Se ratios that are initially ~7:1, decreasing this ratio toward 1:1 causes a dramatic increase in NW branching. In this respect, a Se deficiency empirically sustains the growth of only a single NW from a given catalyst particle. Compensating for this deficiency appears to promote the nucleation of multiple NWs from within individual catalyst NPs, leading to ensembles of branched NWs. A proposed growth mechanism is discussed later.

Figure 4a shows a representative low-resolution TEM micrograph of an ensemble of branched NWs. Three morphologies are commonly observed and are referred to as "tripod", "v-shaped", and "y-shaped" NWs. Characteristic low resolution micrographs of these structures are shown in Figure 4c, e, and g) and corresponding HRTEM micrographs are illustrated in Figure 4b, d, f, and h). The tripods in Figure 4b and c show narrow (~8 nm) arm diameters and lengths between 1 and 10 μm. High-resolution micrographs, such as Figure 4b and d, reveal that both the core and arms of the tripod are crystalline. The core is also ZB and exhibits characteristic lattice fringes of a ZB crystal viewed along ⟨110⟩. Twin boundaries are observed at two of the core/arm interfaces.

Interestingly, HRTEM images of tripod centers consistently show that one of the three arms appears out of focus near the core/arm interface. In Figure 4b, this can be seen in the bottom left arm. Likewise, in Figure 4d, this is evident in the topmost arm (additional examples, Supporting Information). Detailed structural analyses (discussed later), corroborated by such apparent out-of-focus regions, suggest that the third arm extends 54.7° out of the substrate. In contrast, the other two arms lie within the plane of the substrate.

V-shaped NWs are shown in Figure 4e and f. Low-resolution micrographs, such as Figure 4e, again demonstrate that the arms have narrow diameters and lengths between 1 and 10 μm. Corresponding HRTEM micrographs show a ZB core and twinned arms within the substrate plane that exhibit twin boundaries at their core/arm interfaces (additional examples, Supporting Information). Similar behavior is seen in y-shaped NWs shown in Figure 4g and h where a HRTEM analysis shows a ZB core and three arms lying within the plane of the TEM grid (additional examples, Supporting Information). In addition, two of three core/arm interfaces exhibits a twin boundary, similar to tripods. Apart from ZB cores, all tripods, v-shapes, and y-shapes have at least two pointed ends as well as a single flat end (tripods, y-shapes), analogous to those seen in straight NWs. Figure 2c demonstrates this for the case of a tripod NW. The number of flat and pointed ends therefore provides clues for models attempting to explain branched NW growth. In all cases, there appears to be no significant shape selectivity to current branched NW preparations, such that admixtures of tripods, v-shapes, and y-shapes as well as other branched NWs (discussed later) are obtained, as opposed to one exclusive shape.

Further TEM studies of both straight and branched NWs yield structural parameters that are summarized in Figure 5 a–d. Figure 5a shows that straight NWs

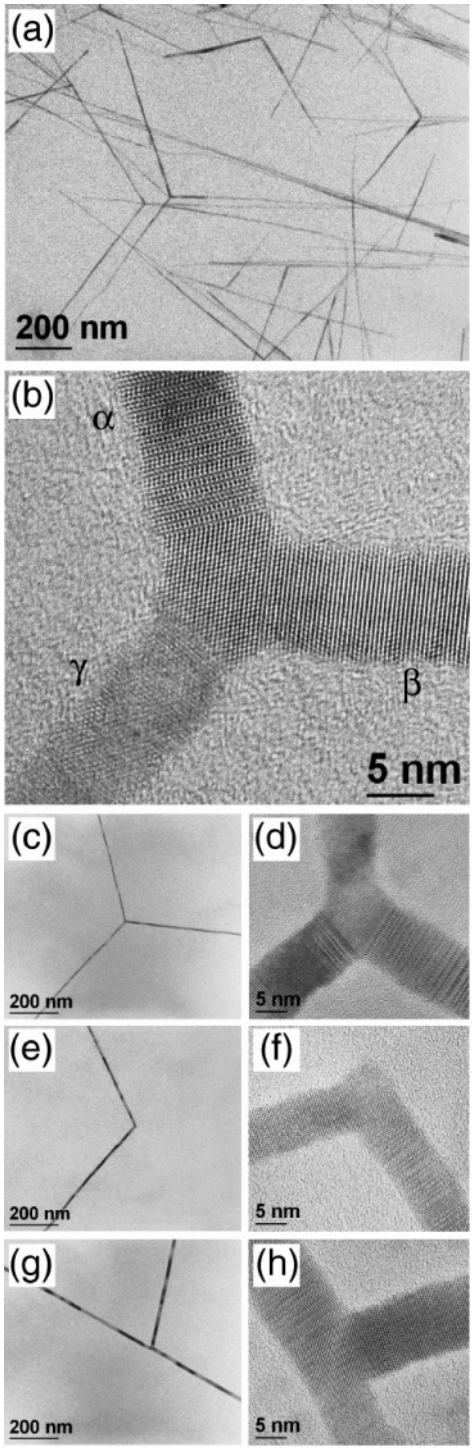

Figure 4. (a) Low-resolution TEM micrograph of branched CdSe NWs. (b) HRTEM micrograph of a tripod NW center. (c) Low-resolution TEM micrograph of a tripod NW. (d) HRTEM micrograph of a tripod NW center. (e) Low-resolution TEM micrograph of a v-shaped NW. (f) HRTEM micrograph of a v-shaped NW center. (g) Low-resolution TEM micrograph of a y-shaped NW. (h) HRTEM micrograph of a y-shaped NW center.

have growth axes which coincide with ⟨111⟩/⟨0001⟩ ZB/W directions.[23,37] Twin boundaries are characterized by a zigzag lattice pattern, apparent when the NW is viewed down ⟨110⟩ directions normal to the growth axis. More often than not, however, twinning is obscured by non ⟨110⟩ orientations such that only parallel lattice fringes are observed normal to the wire axis (Figure 3d).

Tripods (Figure 5b), v-shapes (Figure 5c), and y-shapes (Figure 5d) all exhibit two components: a ZB core and arms that grow out of equivalent {111} ZB faces. The ZB core is analogous to that observed in CdSe tetrapods.[14] Furthermore, each arm in Figure 5, labeled by Greek letters, α, α′, β, or γ, exhibits structural characteristics identical to those of straight NWs, namely growth along ⟨111⟩/⟨0001⟩ directions and twinned ZB sections. Because of the rigid orientation of the arms relative to the core, as well as substrate effects, the orientation of each branch relative to the viewer is typically ⟨110⟩ or ⟨11$\bar{2}$0⟩.

An obvious difference between tripods and y-shapes compared to v-shapes is the presence of a third arm. More subtly though, while tripods and v-shapes exhibit twin boundaries at most (possibly all) core/arm interfaces, y-shaped NWs have a characteristic, missing twin boundary associated with α′ (dashed line, Figure 5d). The α′ arm is therefore unique; not only does it lack a twin boundary but it also grows along the same ⟨111⟩/⟨0001⟩ ZB/W growth direction as α, rather than along a different ⟨111⟩ direction. In contrast, all tripod arms grow exclusively out of different {111} faces. Furthermore, the α′ arm retains the ZB character of the core for a small initial distance down the length of the wire before it reverts to twinned behavior characteristic of straight NWs.

Additional structural parameters describing branched NWs are summarized in Tables 1 and 2. In the case of tripods and v-shapes, previously described TEM lattice images show that the ZB core is viewed down [110]. Arms α and β extend from its ($\bar{1}$11) and (1$\bar{1}$1) faces approximately along [$\bar{1}$11] and [1$\bar{1}$1] (Figure 5b), which are 109.5° from each other and lie within the image plane. Experimentally observed αβ angles of 109° for tripods (σ = 3°) and 110° for v-shapes (σ = 2°) are therefore consistent with this orientation and are summarized in Table 1. The other two {111} planes of the core are inclined with their ⟨111⟩ normals making angles of 54.7° relative to the image plane. In this respect, if the third arm of tripods (γ) grows along one of these directions, its projection onto the (110) image plane will lie along [00$\bar{1}$], which is 125.3° from the idealized [$\bar{1}$11] and [11$\bar{1}$] axes of α and β. Thus, the experimentally measured angles $<\alpha\gamma$ = 124° (σ = 3°) and $<\beta\gamma$ = 127° (σ = 4°) in Table 1 are in excellent agreement with this assumption, strongly suggesting that γ extends out of the (110) image plane.

In addition, if γ has the same structure and orientation as the ZB core, its lattice image will show the same geometry as the center junction. This can be seen in γ near the core/arm interface in Figure 4b, which shows a weak lattice structure image having the same orientation as the ZB center. In general though, experimental HRTEM images usually show only lattice fringes normal to the γ growth axis, as seen in Figure 4d. This behavior is expected if γ is tilted slightly so that only the ZB (002) fringes (3.04 Å spacing) are visible. Similarly, if γ has W sections, its orientation is close to that required for exhibiting W (0$\bar{1}$11) fringes (3.29 Å spacing), which are also normal to the growth axis. In addition, twinned segments of γ are suitably oriented to produce {442} lattice fringes. However, since their spacing is below the resolution limit of the TEM no

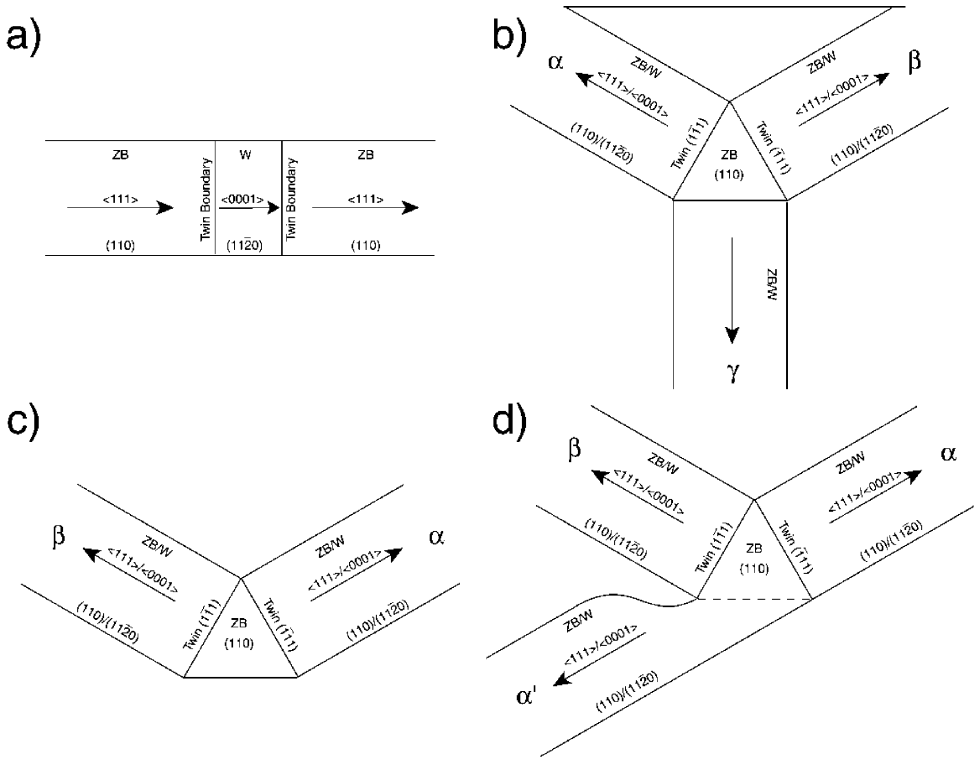

Figure 5. Cartoon showing orientation and growth directions of observed branched NWs: (a) straight NWs; (b) tripod-shaped NWs; (c) v-shaped NWs; and (d) y-shaped NWs. Arms are labeled with Greek letters for convenience.

Table 1. Calculated and Measured Structural Parameters of Tripod and V-Shaped NWs[a]

	$<\alpha\beta_{expt}$	$<\alpha\beta_{calc}$	$<\alpha\gamma_{expt}$	$<\alpha\gamma_{calc}$	$<\beta\gamma_{expt}$	$<\beta\gamma_{calc}$	α/β	α/γ	β/γ
tripod	109° (3)	109.47°	124° (3)	125.26°	127° (4)	125.26°	1.0 (1)	1.1 (1)	1.1 (1)
v-shape	110° (2)	109.47°					1.0 (1)		

[a] Number in parentheses represents one standard deviation in degrees.

Table 2. Calculated and Measured Structural Parameters of Y-Shaped NWs[a]

	$<\alpha\beta_{expt}$	$<\alpha\beta_{calc}$	$<\alpha'\beta_{expt}$	$<\alpha'\beta_{calc}$	α/β	α/α'	β/α'
y-shape	110° (4)	109.47°	69° (3)	70.53°	1.0 (1)	1.3 (1)	1.2 (1)

[a] Number in parentheses represents one standard deviation in degrees.

lattice fringes are expected from these sections. In general, since the twins are only a few atomic layers thick and are inclined relative to the viewing direction such that the electron beam always passes through both twinned and untwinned layers, lattice fringes from untwinned sections are observed. Therefore, the fact that the lattice structure image in Figure 4b is weak is probably due to the presence of such thin twinned segments which do not contribute to the lattice image formed by untwinned sections of γ. Thus, the observation that tripod γ-branch lattice images often appear out of focus is expected and explained. Gradual bending of γ may also contribute to this effect by changing the NW orientation to one generally unsuitable for lattice imaging. HRTEM observations are therefore consistent with tripod γ arm growth along a ⟨111⟩ direction of the ZB core, with the same ZB/W structure as the other two arms.

In the case of y-shaped structures, the angle between α and β is 109.5° (110°, $\sigma = 4°$) with a complementary $\alpha'\beta$ angle of 70.5° (69°, $\sigma = 3°$) (Table 2). This $\alpha'\beta$ angle is rationalized if all arms of the y-shaped NW (α,β,α′) lie within the plane of the substrate and α′ grows along a preexisting ⟨111⟩//⟨0001⟩ growth direction, as suggested by previous HRTEM micrographs. Table 1 also shows that diameter ratios (α/β, α/γ, β/γ) in branched tripods and v-shapes are nearly 1:1. In the case of y-shaped NWs (Table 2), a notable exception to these symmetric arm diameters is α′, which is thinner than either α or β by ∼23% near the core/arm interface.

Apart from the aforementioned tripods, v-shapes, and y-shapes, an additional structure is observed in branched NW preparations. This "merged-y" structure is shown in Figure 6a. It appears similar to a tripod, but has different structural parameters. Rather than 109.5° between different arms, variable $\alpha\beta$, as well as $\alpha\gamma$ and $\beta\gamma$, angles are observed (average $\alpha\beta$ angle 74°, $\sigma = 10°$). This results because no ZB core unites the three arms. Instead, a high-angle grain boundary runs down the length of an apparent third arm labeled γ, preserving the original ⟨111⟩//⟨0001⟩ ZB/W growth directions of both α and β. A representative HRTEM micrograph illustrating this is shown in Figure 6b along with a cartoon in Figure 6c summarizing its known structural parameters.

Further characterization of straight/branched NWs has been conducted through XRD and EDXS analyses. XRD powder patterns were taken on samples consisting of straight, branched, and mixtures of the two types of NWs. Figure 7 shows in all three cases a suppression and enhancement of reflections normally associated

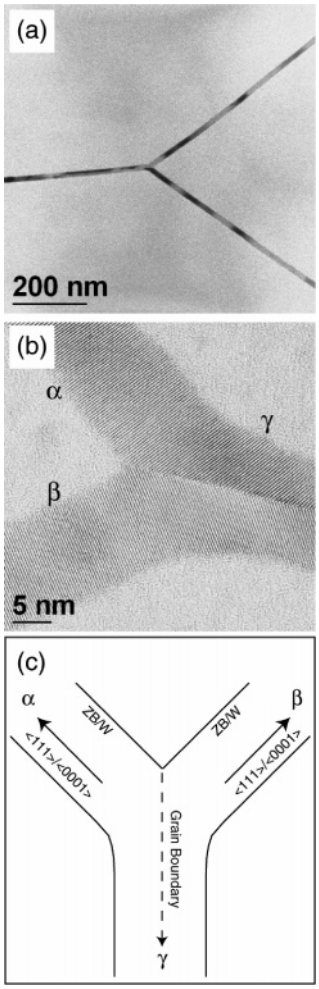

Figure 6. (a) Low-resolution TEM micrograph of a merged-y NW. (b) HRTEM micrograph of a merged-y NW junction. (c) Cartoon depicting the growth directions of the α and β arms in merged-y NWs.

with bulk ZB and W CdSe. These changes are likely caused by substrate-induced NW orientation.[23] In a powder X-ray diffractometer, only planes parallel to the surface produce strong diffraction lines; it is further reasonable to assume that all NWs lie nearly flat on the substrate. Thus, in the case of a ZB wire segment, if the [111] direction corresponds to the growth axis and all wires lie flat on the substrate, only planes parallel to [111] (i.e., members of the [111] zone) diffract strongly. Relevant ZB planes that contribute significantly to the XRD pattern are therefore (220), (422), and (440). Likewise, in the case of a wurtzite NW with a [0001] growth axis, only $(10\bar{1}0)$, $(11\bar{2}0)$, $(20\bar{2}0)$, $(21\bar{3}0)$, and $(30\bar{3}0)$ reflect strongly. In this manner, all peaks both present and absent in Figure 7 can be accounted for. Exceptions to this analysis are the weak shoulders at $2\theta = 49.6°$ and $2\theta = 67.3°$, and the very weak reflection at $2\theta = 97.2°$. These features have corresponding planes with slight deviations from [111] and [0001] such that imperfect NW orientations, a few degrees from being parallel to the substrate, may cause noticeable contributions to the XRD pattern.

Complementary EDXS measurements (Supporting Information) of both straight and branched NWs show statistically equivalent Cd/Se ratios. In particular, an average Cd/Se ratio of 1.4 ($\sigma = 1$) is obtained for both

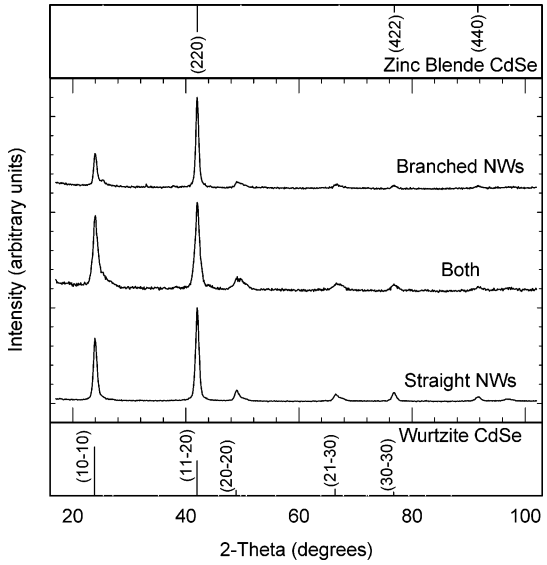

Figure 7. Wide-angle X-ray powder diffraction patterns of straight NWs, highly branched NWs, and an admixture of both types. Stick patterns of the zinc blende and wurtzite phases are provided for comparison purposes. Orientation enhanced lines are depicted in solid black and are indexed. Suppressed lines are shown in gray.

straight and branched NWs. This occurs despite their dramatically different (initial) reaction mixture Cd/Se ratios of ~7.0:1.0 (straight NWs) and ~1.7:1.0 (branched NWs).

Figure 8 shows UV−visible absorption spectra of straight (Figure 8a) and branched (Figure 8b) CdSe NWs. In both cases, a strong absorption edge is seen below the bulk band gap of CdSe (E_g = 712 nm, 1.74 eV). These absorption edges are accompanied by shoulders at higher energies, suggesting the presence of additional quantized transitions, as well as corresponding subbands. The appearance of discrete transitions is in good agreement with the crystallinity of the straight/branched NWs and their narrow radii below the bulk exciton Bohr radius of CdSe (5.6 nm).[4−6] Inhomogeneous broadening of both absorption spectra likely stems from the residual size distribution of the samples, which is on the order of ~25%. In addition, the similarity between the spectra may be rationalized if the optical transitions of branched NWs are dominated by their arms, however, more detailed experiments are required to verify this.

In addition to tripods, v-shapes, y-shapes, and merged-y NWs, higher-order structures occur in samples that exhibit significant branching. They are especially evident in samples that have been prepared using TOP doping. Examples of such higher-order NWs are shown in Figure 9 a−d. Analysis of these NWs reveals complex morphologies that can be understood as linear combinations of the aforementioned tripods, v-shapes, y-shapes, and merged-y NWs. For example, the higher-order NW in Figure 9a can be described as a superposition of two tripods. Similarly, the structure in Figure 9d can be described as a combination of a tripod and a y-shaped NW. An analogous analysis rationalizes the NWs shown in Figure 9b and c. In general, higher-order NWs have diameters and lengths similar to those of branched NWs. They are also crystalline and exhibit identical ZB cores, core/arm interfaces, and branch angles as tripods,

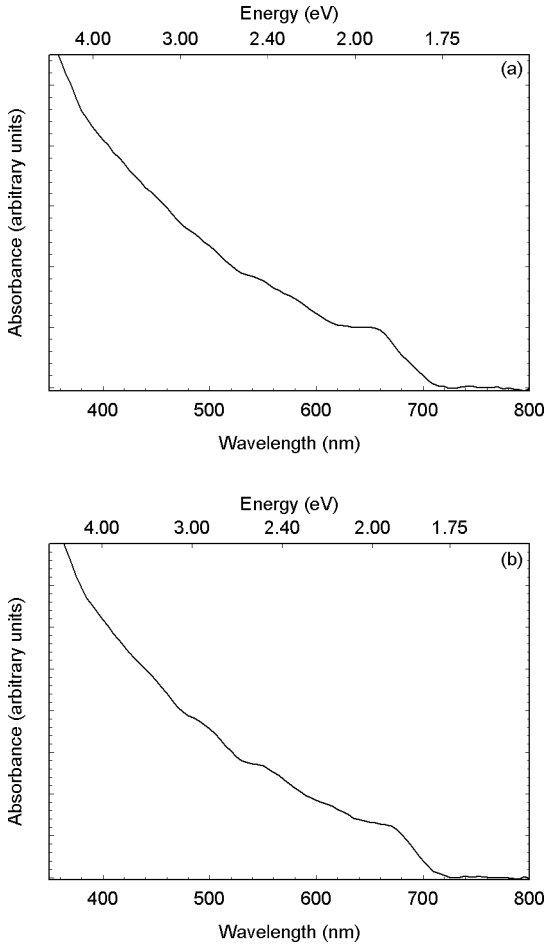

Figure 8. UV/visible absorption spectrum of (a) straight NWs and (b) highly branched NWs in toluene.

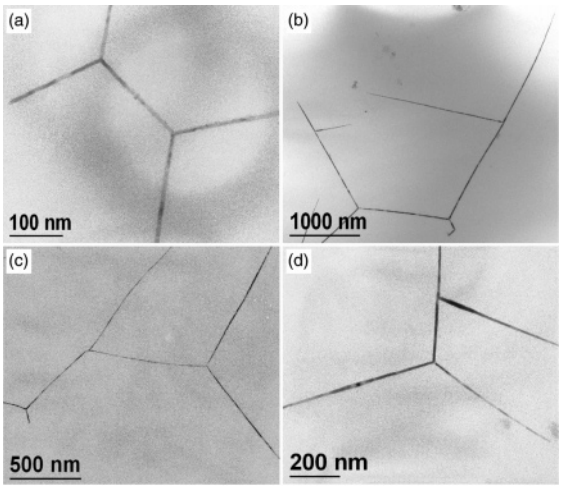

Figure 9. (a)−(d) Low-resolution TEM micrographs of higher-order NWs.

v-shapes, and y-shapes. Furthermore, their intrawire arm diameters vary little such that, overall, higher-order NWs represent an interesting challenge for models aiming to describe the growth mechanism of branched CdSe NWs.

Mechanisms for the Branching. To explain branching as well as the observation of higher-order structures, several potential growth mechanisms are considered. Their successes and failings in explaining straight/branched NW growth are described in succession below.

Uncatalyzed Growth. At its heart, this mechanism assumes that straight or branched NWs can be grown in the absence of catalyst NPs. This assumption is motivated by the observation of solution-based NRs and other quasi-0D structures such as tetrapods with lengths up to ∼100 nm.[12,14] The hypothesis therefore posits uncatalyzed (straight) NW growth as well as branched growth, which occurs when a NW zinc blende section becomes large enough to support branching out of equivalent {111} faces.

Direct control experiments to address this mechanism, however, indicate that catalyst particles are needed to promote NW inception. Furthermore, field emission scanning electron microscopy (FESEM) experiments (Supporting Information) show that at most three arms grow out of a ZB core. By contrast, NWs undergoing uncatalyzed growth might be expected to exhibit four arms, analogous to those observed in tetrapods.[14] These direct and indirect controls therefore suggest that uncatalyzed growth does not appear to be responsible for either straight or branched NWs in the current preparation.

Catalyst Fission. A catalyst fission mechanism requires the Au/Bi NP to split upon saturation. V-shaped NWs are obtained when the NP splits into two; tripod (or y-shaped) NWs result when the catalyst splits into three. Each segment subsequently grows away from the others at fixed angles of 109.5° (the angle between corresponding ⟨111⟩ directions), yielding the physical parameters listed in Tables 1 and 2. Subtle variations in the fission mechanism, such as delaying the point where the NP splits or introducing variable growth angles, can be incorporated to better match the experimental data, and in particular, the observation of merged-y NWs.

However, a fission mechanism fails to explain a host of experimental observations. For example, assuming that the NP alloys/splits, it is not apparent that there should be at most three arms (tripod, y-shaped, merged-y) arising from a given branching point. In principle, the NP may be expected to split into multiple fragments, yielding "sea urchin"-like structures similar to those described by Korgel[24] or even Ellis.[18] Furthermore, *symmetric* NP fission yielding branched NWs with nearly identical arm diameters is highly coincidental (Tables 1 and 2); such problems are even more poignant in the case of higher-order NWs where branch diameters again vary little. Angles between different arms should also be random, whereas v-shaped, y-shaped, and tripod NWs consistently exhibit angles of 109.5°. Finally, blunt NW ends are often associated with the former presence of a Au/Bi NP provided that they are not artifacts due to NW fracture. A fission mechanism therefore predicts v-shaped, y-shaped, merged-y, and tripod NWs with flat ends since each arm undergoes catalyzed growth. This contradicts experimental results, which show that all such NWs exhibit at least 2 pointed ends (Figure 2c).

Collision Mechanism. A collision mechanism assumes that the chance encounter between two (or more) Au/Bi catalyzed wires will lead to a branched NW. Growth either stops to give v-shaped wires or continues, resulting in tripod, y-shaped, or merged-y structures. Alternatively, such tripods, merged-y, or y-shapes can

Scheme 1. NW branching pathways

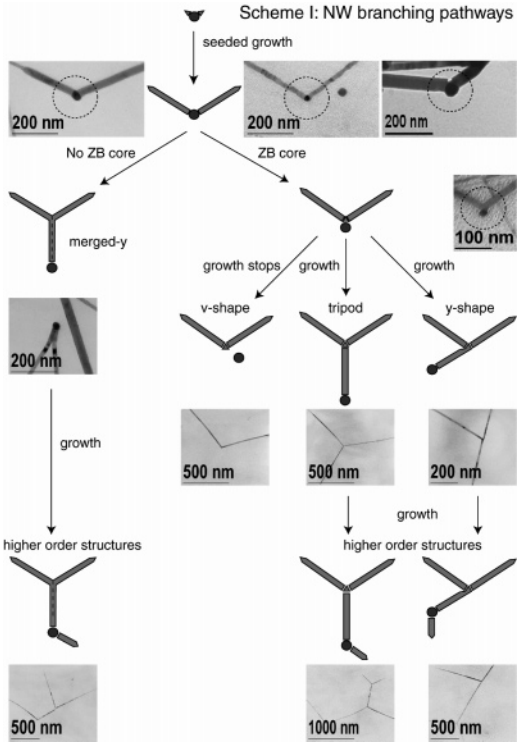

arise from the random encounter of three straight NWs, albeit more infrequently. Higher-order NWs can be rationalized in a similar fashion.

Since a collision mechanism requires growing NWs to meet, concentrating the reaction mixture might, in turn, increase the overall degree of branching in either straight or branched NW preparations. However, as demonstrated earlier, concentrating the reaction mixtures does not discernibly increase branching but instead promotes the growth of QDs at the expense of NWs (self-nucleation versus catalyzed growth). Furthermore, the collision mechanism does not explain the 109.5° angles between different NW arms (Tables 1 and 2), nor does it explain their similar diameters. In principle, a collision mechanism might predict random angles, as well as diameter distributions consistent with the size distribution of the entire NW ensemble (~25%). Thus a mechanism based on random encounters does not explain NW branching in the current synthesis.

Geminate NW Nucleation. A geminate nucleation mechanism suggests that multiple NWs form on the surface of a given Au/Bi NP when sufficient Cd and Se are present in the system to achieve not only supersaturation, but also the growth of more than one arm. This hypothesis is consistent with observed increases in branching within preparations where the Cd/Se ratio approaches 1:1, compensating for a Se deficiency employed in straight NW preparations (Experimental Section). A geminate nucleation mechanism is further corroborated by direct TEM imaging of instances where two NWs appear to originate from a single catalyst particle (top, Scheme 1). The geminate branching mechanism therefore begins to explain a number of experimental observations and also has the appealing feature of rationalizing, in a self-consistent fashion, the observed variety of branched NWs.

We propose that following nucleation, the geminate pair merges to form a branched NW. Initially, the nucleated wires are small but they eventually grow to a size larger than the diameter of the catalyst NP. This is consistent with their pointed ends (Supporting Information) and eventual diameters between 7 and 10 nm. When NW widths match the NP diameter, the two wires touch and form a grain boundary unless their mutual angle exceeds a critical value. In general, the two nucleated wires need not be separated by 109.5° nor must they have parallel ⟨110⟩ orientations. However, on a liquid NP surface, the wires can orient by a process that includes surface diffusion along the grain boundary, easy motion on a liquid NP surface, and on-axis rotation to form a single-crystal ZB junction that connects the two arms.

In this fashion, the surface energy of the initial grain boundary can be eliminated, resulting in characteristic $\alpha\beta$ angles of 109.5° as well as parallel ⟨110⟩ orientations. Next, assuming that a common ZB core unites the two arms, v-shaped, y-shaped, and tripod morphologies can be obtained from additional growth which exposes the ZB junction, expelling the NP catalyst (right pathway, Scheme 1 and Figure 4b, d, and f). The only difference between such branched structures then appears to be continued growth along a third distinct ⟨111⟩ direction for tripods, growth along an existing ⟨111⟩ direction for y-shaped wires, and terminal growth in the case of v-shaped wires, leading to the NP falling off the NW.

Alternatively, in the absence of a ZB core, the two nucleated arms fuse together through a high-angle grain boundary (left pathway, Scheme 1 and Figure 6b) yielding merged-y NWs. Persistence of this initial grain boundary likely occurs when the wires are nucleated so close together on the NP surface that too much rotation is required to eliminate it. This hypothesis is further supported by the fact that merged-y structures always have $\alpha\beta$ angles much less than 109.5° (average $\alpha\beta$ angle 74°, $\sigma = 10°$). Finally, to explain higher-order structures, all tripod, v-shaped, y-shaped, and merged-y NWs retain their catalyst NPs and continue growing. Nucleation of additional arms on the NP surface during this step results in higher-order structures (bottom of Scheme 1 and Figure 9).

Since NW arms originate from the same catalyst particle, their diameters need not vary greatly. This is consistent with the reported distributions in Tables 1 and 2. Growth out of equivalent {111} faces of a ZB core also explains the fixed 109.5° angles between different branched NW arms. The absence of a fourth arm might originate from surface energy considerations where the growth of three arms is thermodynamically stable whereas a fourth arm introduces instability preventing the growth of tetrapod NWs. Furthermore, since only one catalyst NP is involved in the growth of both branched NWs and higher-order structures, the mechanism also predicts the correct number of experimentally observed blunt (one) and pointed (at least two) tips. This, as well as direct TEM observations of catalyzed NW pairs, suggests that a geminate NW nucleation mechanism is responsible for branching and begins to explain, in a self-consistent fashion, the rich variety of branched nanostructures seen in the current preparation.

Conclusion

The work presented herein describes the synthesis and characterization of solution-grown straight and branched CdSe NWs. Using low-melting Au/Bi NPs, the growth of highly crystalline, narrow diameter (<10 nm) NWs with lengths between 1 and 10 μm is achieved. Manipulating the Cd/Se ratio in the solution as well as other reaction conditions such as an excess of trioctylphosphine allows a transition from straight to branched morphologies, leading to v-shaped, y-shaped, merged-y, tripod, and higher-order NWs. Detailed characterization through HRTEM analysis reveals both ZB and W sections along NWs, closely spaced twin boundaries within ZB sections, ⟨111⟩/⟨0001⟩ growth directions, ZB cores, and twin boundaries at their core/arm interfaces. Further analysis of the data suggests that branching is consistent with a geminate NW nucleation mechanism, in agreement with observed structural parameters such as branching angles and diameter distributions. These straight and branched NWs exhibit confinement effects, and in turn, may possess novel optical, electrical, and transport properties. The current solution-based approach for the synthesis of straight, branched, and higher-order NWs adds to a growing body of knowledge about the preparation of solution-based semiconductor NWs and may suggest future ways for developing other quasi-1D materials. These straight and branched CdSe NWs represent systems by which the size- *and* shape-dependent properties of confined 1D and quasi-1D materials can be investigated, further advancing CdSe as a model system for studying the mesoscopic properties of low-dimensional materials.

Acknowledgment. We thank the University of Notre Dame, the Notre Dame Radiation Laboratory, and the Office of Basic Energy Sciences of the U.S. Department of Energy for financial support and for use of their facilities. We also thank A. Khandelwal and A. Imre for assistance with the field emission SEM measurements as well as F. V. Mikulec for assistance with TEM-based EDXS measurements. This is contribution 4537 of the Notre Dame Radiation Laboratory.

Supporting Information Available: Autocorrelation analysis of twinning through contrast in HRTEMs of straight CdSe NWs; additional HRTEM micrographs of branched CdSe NWs; energy-dispersive X-ray spectra of straight and branched CdSe NWs; field emission SEM images of branched NWs (pdf). This material is available free of charge via the Internet at http://pubs.acs.org.

CM048498H